First Results from a Deep Spectroscopic Survey of Faint Red Galaxies - Clues on the Nature of Low Redshift Dwarf Galaxies

L. Tresse, F. Hammer, O. Le Fevre, D. Proust

Astron. Astrophys. 277, 53–61 (1993)

ASTRONOMY AND ASTROPHYSICS

First results from a deep spectroscopic survey of faint red galaxies: clues on the nature of low redshift dwarf galaxies*

L. Tresse[1], F. Hammer[2], O. Le Fèvre[2], and D. Proust[1]

[1] DAEC, Observatoire de Paris-Meudon, F-92195 Meudon Principal Cedex, France
[2] Canada-France-Hawaii Telescope Corporation, P. O. Box 1597, KAMUELA, HI 96743, USA

Received November 5, 1992; accepted March 15, 1993

Abstract. Deep multi-object spectroscopy of a sample of 44 faint galaxies selected on deep I band images is presented. The combination of long integration times with careful data reduction has led to a completeness in redshift measurement of 93 % to a limiting magnitude $I=22.1$. Although we have selected our galaxies from their old stellar content we confirm the existence of an over-abundant population of dwarf galaxies at low redshifts, which are probably responsible for the excess in the blue number counts. Combined with a slight deficiency of high-z galaxies (no galaxies beyond $z=1$), our data provide red counts apparently consistent with an absence of luminosity and number evolution.

Most of the low redshift dwarf galaxies in our sample are star-forming galaxies which is an indication of a high level of activity at relatively low redshifts. We present the discovery of a dwarf galaxy at $z=0.21$, seemingly forming its first generation of population II stars, making it one of the best primordial galaxy candidate. Evidence for galaxy–galaxy interactions in several other dwarfs is presented, especially in the most active ones. We finally stress that differences between red and blue counts result from a complex mixture of effects which will have to be studied from a much larger spectroscopic sample.

Key words: galaxies: compact – starburst – interactions – cosmology

1. Introduction

Since the pioneering work of Tyson (1988), the origin of the excess of faint blue galaxies has been at the center of active debates. This excess was initially attributed to evolved massive high-redshift galaxies in order to preserve the galaxy number density. However, spectroscopic surveys of B-selected samples have provided surprisingly low redshifts (Broadhurst et al. 1988; Colless et al. 1990, 1992; Cowie et al. 1992), generally consistent with scenarios without luminosity evolution, especially for the brightest galaxies. Currently, the blue excess is attributed to galaxy evolution at low redshifts, although there is no clear agreement on which physical processes are dominating (see Cowie et al. 1992, for a review).

Binggeli et al. (1988) have convincingly shown that the luminosity function of field galaxies is the result of the superposition of several type-dependent luminosity functions (E/S0, spirals, dE, Irr, etc.). It now seems that the luminosity function has a different shape for different galaxy types, and differences in the corresponding dynamical properties should yield different time-scales for their evolution. For instance, the first deep spectroscopic surveys (Broadhurst et al. 1988; Colless et al. 1989) show that L^* E/S0 galaxies have undergone little or no evolution since $z=0.7$. More recently, deeper surveys (Cowie et al. 1992; Lilly 1992) show that the excess of blue galaxies is probably due to an evolution of the low end of the luminosity function, populated by either dE, Sdm or Irr galaxies.

Therefore, we believe that the only way to understand the mechanism of galaxy evolution is to build a complete sample of faint galaxies which satisfies the following conditions: (i) a sufficiently large number of galaxies in order to characterize their types or their intrinsic colors (3 to 5 type-bins), their luminosities (3 luminosity-bins per type) and their redshifts (3 evolution-bins per type and luminosity); several tens of galaxies are needed in each bin (type-luminosity-redshift), and this leads to the requirement of a sample with one thousand galaxies or more, (ii) a careful photometric analysis of the fields prior to object selection for spectroscopy, to gather an unbiased sample down to a low surface brightness ($\mu_I=26.5$ mag arcsec^{-2}), (iii) a spectroscopic limit reachable in less than 8 h with a 4 m class telescope and compatible with at least a 90% completeness, (iv) a selection of the galaxies in a photometric band within reach of the spectroscopic instrumentation and as red as possible to sample the light emitted at

Send offprint requests to: F. Hammer

* Based on observations obtained with the Canada-France-Hawaii Telescope, operated by the NRC of Canada, the CNRS of France and the University of Hawaii.

$\lambda > 4000$ Å generally related to the mass of the old stellar population; an I band selected sample is then quite attractive (also because I-selected galaxies are less sensitive to K-corrections and their related uncertainties), (v) more than three fields to select the galaxies corresponding to independent lines of sight ($b_{II} > 50°$). We present here the first results of a larger scale survey.

2. Observations

2.1. Deep photometry

Four high galactic latitude fields have been selected for this program and are listed in Table 1. Deep imaging has been performed in November 1991 and January 1992 at the CFHT prime focus with FOCAM and the Lick 2 2048×2048 pixel^2 CCD. Areas of 10×10 arcmin^2 have been covered by 4 one hour long integrations in the I band, each covering 7×7 arcmin^2 with a scale of 0.2 arcsec per pixel. As a result of the paving on the sky, the 10×10 arcmin^2 areas are made of 9 areas with the central 4×4 arcmin^2 totalling 4 h of integrations, while the outer corners total 1 h. The image quality was measured on stars in each frame between 0.7″ and 1.0″ FWHM, and the conditions were photometric both in November and January. V and R band images have also been obtained for some of the fields under similar conditions.

Objects were identified with the FIND routine in DAOPHOT with a low intensity threshold which identifies most real objects and an additional 30% false objects. From there, we followed two independent schemes. First, a similar list was produced for the V bandpass, and a list of objects common to V and I frame was created. Then visual inspection on the I frame was carried out to add those objects not in the correlated list, i.e. objects being detected in I but not in V. The second scheme was to inspect visually the I frame and to delete from the initial list what appeared as false detections, and add the objects not picked up by the FIND routine. These two schemes produced virtually identical lists of detected objects which are basically threshold limited to objects with central surface brightnesses brighter than I surface brightnesses ranging from $\mu_I = 26.3$ (1 h) to $\mu_I = 27$ (4 h). The photometry of all objects in the frames was then performed with the faint galaxy photometry package GALPHOT (Le Fèvre et al. 1986; Le Fèvre 1993, in prep.). It consisted of the following steps for each object: (1) Compute centroids and ellipse fitting for each object, (2) compute a one dimensional photometric profile after eliminating nearby objects, (3) compute the final photometric parameters: position, isophotal radius, ellipticity, position angle, central surface brightness, isophotal I magnitude. Two isophotal magnitudes were computed, in the isophotes $\mu_I = 27.5$ mag arcsec^{-2} and $\mu_I = 28$ mag arcsec^{-2}. This latter allowed to assess the fraction of a galaxy's flux that was missed by using isophotal magnitudes measurements. Simulations showed that at the spectroscopic limit, and at the photometric detection limit, the $I_{27.5}$ magnitude is nearly identical to a total magnitude measurement (Le Fèvre 1993, in prep.). The limiting magnitude of the sample is typically $I_{27.5} = 24.5$, while we estimate the magnitude of completeness to be $I_{27.5} = 23.5$. Photometric catalogs containing around 2000 objects per survey field were finally produced. No attempt was made to select stars from galaxies, as we wished not to exclude compact galaxies and QSOs from our survey. The internal photometric error is expected to be less than 0.05 mag for $I \leq 22.1$, while a photometric zero point error was computed to be less than 0.06 mag from the observation of multiple standard stars.

2.2. Deep multi-object spectroscopy

2.2.1. Object selection

To ensure a maximum spectral coverage, we selected targets for spectroscopy in sky strips 20″ wide and 6′ long. Objects within these strips and with $I_{27.5} \leq 22.5$ were first selected. Then from this list, aperture masks with slits of width 1.5″ and minimum length 13″ were designed in order to maximize the number of objects per aperture mask. We did not intend at this stage to ensure completeness in spatial coverage, and therefore the present observations are ill-suited for large scale structure studies. The magnitude distribution of the spectroscopic sample follows the distribution of the photometric sample.

2.2.2. Observations

The spectroscopic observations were carried out on the nights February 5 to 8, 1992. We used the MARLIN focal reducer with the SAIC1 CCD, providing a plate scale of 0.34 arcsec per pixel and a readout noise of 9 e$^-$. On the first night deep images were acquired to identify the preselected objects and design the aperture masks which contained an average of 20 slits of 1.5″ width and minimum length of 12″. Mask cutting was performed using the LAMA laser machine, providing better than 2 μm rms residual cutting irregularities on the slits edges. Mask positioning was quickly performed due to our care to include a 3″ diameter centering hole on a bright star for each mask (one star is adequate since no rotational adjustment is necessary with the instrumental set-up used). Field centering and mask positioning was constantly checked between successive 1 h exposures to avoid drift associated to instrument flexures. Three fields were observed: F0300-00 for a total of 6 h with the O300 grism (17 Å resolution, spectral range 4500–8500 Å); F0958+255 for a total of 7 h with the O300 grism; and F1416+527 for 7 h with the R150 grism (34 Å resolution, spectral range 4200–9000 Å). The image quality was measured on field acquisition images between 0.75″ and 0.9″ all along the observations and the conditions were photometric except for the first night

Table 1. Coordinates of survey fields

Field	α_{1950}	δ_{1950}	b_{II}
0000+00	0^h00	0°00	−60°
0300−00	3^h00	0°00	−50°
0958+26	9^h58	26°00	+60°
1415+52	14^h15	52°00	+50°

with some cirrus. Calibration exposures were taken throughout the night, including the observation of the spectrophotometric standard stars HZ44 and Feige 15 (Oke 1974), bias exposures, white light images of the aperture masks, quartz lamp spectra and He+Ar wavelength calibration spectra through the aperture masks.

The use of two different spectral resolutions, 17 and 34 Å with the O300 and V150 grisms respectively, was quite informative. It turns out that the field observed with the lowest resolution did yield a 100% redshift measurement completeness, i.e. better than the two other fields observed at the higher resolution. Although we are dealing with small numbers we think that this is a good indication that spectra with 30 Å resolution are quite suitable for a deep redshift survey. This has important implications for the total number of objects one can fit per aperture mask, and therefore on the efficiency of the survey.

2.2.3. Data reduction

The data were processed using a highly efficient tool designed for multi-object spectroscopy at CFHT, in the form of an IRAF script based upon tasks in the LONGSLIT package which treats each slitlet in the same way as a long slit would be (Le Fèvre et al. 1993, in prep.). Each 1 h spectrum for each slit was first processed in the following way: (1) bias subtraction of the corresponding area, (2) flat fielding from the fit of the corresponding quartz lamp spectrum, (3) sky spectrum subtraction. The sky spectrum subtraction was done by fitting pixel intensities perpendicular to the dispersion line by line using the IRAF task BACKGROUND with spline1 functions of order 2 or spline3 with order 1. It proved to be of high quality up to 9000 Å (Fig. 2), with residuals 0.2–0.5% of the sky intensity. We attribute this to the high quality of the laser cutting, the adequate number of spatial pixels per slitlet (>40) and the SAIC1 CCD cosmetic, low noise and no fringing qualities. The 1 h sky corrected spectra were then combined for each slitlet with an average sigma clipping algorithm which removed most of the cosmic ray events. One dimension spectra were finally produced by extraction from the 2D spectra using the IRAF/APSUM task and were then calibrated in wavelength and flux.

3. The data

3.1. Photometric depth and completeness

Our selection process ensures that the spectroscopic sample adequately samples field galaxies down to $I=22.1$. Number densities and corresponding slopes of the galaxy counts (up to our photometric completeness, $I=23.5$) observed in our three fields are consistent with previous data (Lilly et al. 1991 and references therein), although one field (0958+25) shows a number excess of 30% when compared to other fields. Examination of this field does not reveal the presence of a galaxy cluster. The magnitude distribution of our spectroscopic sample is also consistent with the slope of galaxies counts. Since both aperture and isophotal magnitudes lead to an underestimate of the total luminosities, especially for low-surface brightness objects, we have chosen to estimate relative luminosities of our sources using isophotal magnitudes, which have, in our view, the advantage of an integration radius closely tuned to the spatial extent of the galaxies. For a $I=22$ galaxy with an exponential luminosity profile with $r_{disk}=5$ kpc ($H_0=50$), the isophote $m_I=27.5$ mag arcsec^{-2} includes 98% of the "total" luminosity, if the galaxy is assumed at $z>0.5$, while a deeper isophotal limit ($m_I=28$ mag arcsec^{-2}) allows to include only 1% more of the light. The fraction of measured light decreases to only 95% when assuming $r_{disk}=10$ kpc ($H_0=50$). Note that this amounts of "missed" light is of same order as measurement errors (0.05 mag at $I=22$). This corroborates a similar study by Colless et al. (1992), who found that only very small selection effects (associated to surface-brightness dimming) can be expected for high-z galaxies. Very low surface-brightness sources should correspond to very low-z galaxies which should be rather rare in such small field areas. We would still detect 95% of the light from dwarf galaxies at $z=0.1$ if they had $r_{disk}<1.8$ kpc. As described in Sect. 2.1, we have adopted two isophotal magnitudes, and found that less than 98% of the objects selected from $I_{iso=28}$ magnitudes are also selected from $I_{iso=27.5}$ magnitudes: at our magnitude limit, less than one object might be missed because of using the $I=27.5$ mag arcsec^{-2} isophote instead of 28.

3.2. Redshift measurements and spectroscopic completeness

Redshift measurements have been carried out independently by two groups of our team. Emission lines in the one dimensional spectra have been confirmed on the 2D spectra, to avoid confusion with residuals of cosmic rays or sky line correction. We have used both visual and correlation techniques, the latter being performed with the Harvard-CfA/RVSAO routine and a package designed under the EVE environment at the Observatoire de Paris-Meudon, with several templates successively correlated to each object. Redshift measurements of each group have been then compared, and found in excellent agreement,

with differences for less than 10% of the objects. These have been later re-examined, to assign or not a final redshift. Table 2 presents the list of the 44 galaxies (4 stars) brighter than $I=22.1$, and their corresponding magnitudes and redshifts. Three objects have no redshift assigned, due to the lack of evident features. It yields a 93% spectroscopic completeness for our survey (92%, 90% and 100% in the fields 0300+00, 0958+25 and 1415+52, respectively). All the other 41 objects have been found to have two or more features (emission or absorption), including the 4 stars. Redshift distributions derived from individual fields are consistent from one another, and their differences can be related to their incompleteness. Comparing one field with another with a Student's t-test, we found that the redshift distributions were only marginally different.

4. General properties of $I \leq 22.1$ galaxies

4.1. Redshift distribution

The redshift distribution of our 41 identified galaxies has an average value $\langle z \rangle = 0.561 \pm 0.25$ a median of $z=0.63$, and the highest redshift is 0.994 (Fig. 1). The F0958+25 field sample has the highest average redshift ($\langle z \rangle = 0.63$) as well as the highest degree of incompleteness, while the 1415+52 is exactly in the opposite situation ($\langle z \rangle = 0.49$). This might indicate that unidentified objects have rather low redshifts. However if all unidentified objects were assumed at $z=0$, $\langle z \rangle$ would decrease only to 0.511 (it would increase to 0.598 for $z=1$) and therefore the incompleteness is not expected to significantly affect our results.

4.2. Excess of low-luminosity dwarf galaxies

The sample of 22 $B \leq 24$ galaxies from Cowie et al. (1992) provides a significantly lower average redshift ($\langle z \rangle = 0.380 \pm 0.176$) than ours. The probability that both samples are drawn from the same redshift distribution is smaller than 0.5 % from a Student's t test. From Fig. 6 of Lilly et al. (1991), only one-half of the galaxies which verify $B \leq 24$ or $I \leq 22.1$ also verify $B \leq 24$ and $I \leq 22.1$. It implies that the bluest galaxies ($B-I \leq 1.9$) should lie at much lower redshifts than the reddest ones, a rough estimate giving a $z=0.5$ difference between the two populations. This is consistent with the idea that most of the faint blue galaxies are dwarfs lying at relatively low z ($B \simeq 24$ and $z \simeq 0.25$; see Lilly et al. 1991; Cowie et al. 1992), while only a fraction of them are bright enough to enter our I-limited sample. These dwarfs would be responsible for the excess of blue galaxies in the counts, at least up to $B=24$, while red counts present no excess.

The existence of an overwhelming population of dwarfs is also supported by the redshift distribution in our sample as shown in Fig. 1, where we also show the distribution expected by assuming that the local luminosity function (f^* and M^* quoted by Efstathiou et al. 1988) characterizes the galaxy population up to $z=1$ or more (a hypothesis that we improperly name no-evolution scenario).

Although the distribution is very close to the no-evolution scenario, there are significant differences at both low and high redshift ends. No galaxies with $z \geq 1$ were found, but comparison with any model is difficult, because at high-z uncertainties related to K-corrections or to cosmological parameters become very high. Low luminosity galaxies selected at red-wavelengths are dwarfs with respect to their old stellar content. We find a significant excess of dwarf galaxies at low-z compared to the no-evolution scenario. Two galaxies have $L \leq 0.01 L^*$, and 5 have $L \leq 0.025 L^*$, while the no-evolution scenario predicts only 0.2 and 1, respectively. Figure 1 shows that this excess could not be affected either by uncertainties related to K-corrections, which should be small for low-z galaxies, or by cosmological parameters. While the local luminosity function fits well moderate luminosity galaxies ($L > 0.05 L^*$), there is a 3σ excess of $\simeq 0.01$–$0.02 L^*$ galaxies.

Table 2. Magnitudes and redshifts of the sample galaxies

(1)	(2)	(3)	(4)	(5)	(6)	(7)	(8)	(9)
Field 0300+00								
1	148	362.0	449.8	18.60	18.01	0.0000	5	M star
5	907	320.6	388.5	22.85	21.72	0.5047	2	CaH, CaK, G, SED
7	837	304.0	339.3	22.93	21.29	?	0	Not enough flux
7	825	303.4	333.9	22.38	21.61	0.7870	2	[O II], CaH
8	806	304.4	325.6	22.14	21.55	0.7518	2	[O III], CaH, SED
9	767	300.8	303.5	24.11	21.17	0.6690	3	[O II], CaH, break 4000 Å
10	743	302.2	283.7	21.23	18.73	0.4657	5	CaK, CaH, Hβ(a)
11	726	318.1	272.3	22.20	21.31	0.1351	5	[2*O III], Hβ, Mg I, O I, Hα
12	711	323.6	259.3	21.93	20.56	0.3137	2	CaK, CaH, SED
13	692	279.2	246.7	21.25	19.98	0.1830	2	Hα, [N II]
16	620	297.7	190.5	24.26	22.02	0.8320	3	[O II], CaK, CaH
17	1349	320.5	157.2	21.86	20.39	0.6155	4	[O II], [Ne III], CaK, CaH(?), [O III]
19	1318	318.2	129.5	22.84	21.81	0.8575	2	[O III (3133 Å)], [O II]

Table 2 (continued)

(1)	(2)	(3)	(4)	(5)	(6)	(7)	(8)	(9)
Field 0958+25								
1	2183	371.6	127.0	22.93	20.97	0.9106	2	[O II], [Ne III (?)], SED
2	2197	368.9	149.1	21.81	21.34	0.3830	2	[O II], Hδ(a), Hβ(a), [2*O III]
4	2215	391.1	174.6	21.45	19.94	0.7300	2	CaK, CaH, G, SED
5	2224	368.4	180.7	22.80	21.59	?	0	Not enough flux
7	1105	390.7	222.2	22.40	21.87	0.7770	4	[O II], CaK, CaH, break 4000 Å
8	1116	399.9	233.2	22.27	21.23	0.7090	2	[O II], CaK, CaH, break 4000 Å
9	1135	380.6	247.7	22.89	21.65	0.7290	3	[O II], [Ne III], break 4000 Å
10	1155	262.6	262.6	21.48	20.62	0.5074	5	[O II], Hβ, [2*O III]
11	1182	404.3	284.0	23.04	21.99	0.4670	2	[O II], CaK, CaH, SED
13	1236	382.6	315.3	22.44	21.54	0.7498	3	[O II], CaK, CaH, SED
14	1262	384.2	331.9	21.72	21.04	0.5775	5	CaK, CaH, Hδ(a), [O III]
15	1281	370.2	342.5	22.39	21.21	0.1112	3	Hβ, He II, Hα
16	1313	371.3	359.0	22.53	21.66	?	0	Not enough flux
17	1349	386.6	389.9	21.29	19.70	0.4681	4	CaK, CaH, [He II], break 4000 Å
17	1423	385.7	393.1	23.07	21.99	0.7242	2	[O II], CaK, break 4000 Å
18	1370	399.1	409.7	22.22	21.01	0.6770	2	[O II], CaK, break 4000 Å
19	1379	409.6	417.1	21.35	20.51	0.4980	2	[O II], G, SED
20	169	391.7	442.7	22.84	22.07	0.9935	5	[O II], [Ne III], Mg II
21	178	402.2	448.7	20.23	19.52	0.5523	5	CaK, CaH, Hδ, G
Field 1415+05								
1	2632	197.0	140.0	23.88	21.97	0.0670	5	Hβ(a), [O III], Hα, [S II]
3	1591	203.2	168.9	23.71	21.92	0.6580	3	[O II], Hδ, Hβ, G, [O III]
3	638	203.0	182.6	20.20	19.75	0.0000	5	M star
7	726	208.6	237.7	23.32	21.94	0.2330	4	[O II], Hγ(?), Hβ, [2*O III], He I, Hα
8	772	222.8	260.2	21.85	20.90	0.4770	3	[O II], CaK, Hδ(a), G(?), Hβ, [O III]
9	789	220.1	271.6	21.92	21.17	0.9877	3	[O II], CaH, break 4000 Å
10	809	205.9	284.9	22.87	21.96	0.3607	3	[O II], [2*O III]
11	825	218.0	297.5	21.98	20.87	0.5495	3	[O II], [Ne III], CaH, Hδ(a), Hβ
12	847	216.8	313.3	21.71	20.92	0.7205	3	[O II], [O III], SED
13	880	211.1	331.9	18.50	18.04	0.0000	5	Star
14	550	187.0	341.3	23.17	22.03	0.6722	3	[O II], [Ne III], CaK, CaH
16	961	207.6	380.5	22.77	21.61	0.9003	2	[O II], SED
17	577	177.7	390.1	21.80	20.92	0.4345	2	CaK, CaH, break 4000 Å
19	153	201.3	427.7	19.18	18.78	0.0000	5	M star
19	1027	198.7	422.4	23.46	21.91	0.2250	5	[2*Ne III], Hδ, Hγ + [O III (4363 Å)] He I, He II, Hβ, [2*O III], Hα
20	164	222.7	446.9	20.89	18.79	0.0806	5	Hβ, [2*O III], He I, O I, Hα, [S II], [O II]

(1) And (2): Spectroscopy and photometry identification numbers
(3) And (4): Position X and Y in arcsec
(5) Central surface brightness in mag arcsec^{-2}
(6) $I_{27.5}$ isophotal magnitude in the $I=27.5$ mag arcsec^{-2} isophote
(7) Redshift
(8) Number of features identified in spectrum
(9) Features identified, Hδ(a) and Hβ(a) for absorption lines

Table 3 lists the properties of the 6 dwarfs ($L \leq 0.05L^*$) found in our survey. Most of them verify $B-I \leq 1.9$ and therefore have a rather flat spectrum. Half of them are so blue that they would even belong to a $B \leq 22.5$ sample. Moreover, the excess of dwarfs that we found at red wavelengths may be of the same order than the excess of blue galaxies in spectroscopic and photometric counts.

5. Nature of the over-abundant population of dwarf galaxies

5.1. Star forming galaxies

The 6 dwarf galaxies have redshifts between $z=0.06$ and $z=0.25$. All of them show Hα in emission (Fig. 2), a property shared by all the $z<0.3$ galaxies of our sample (for

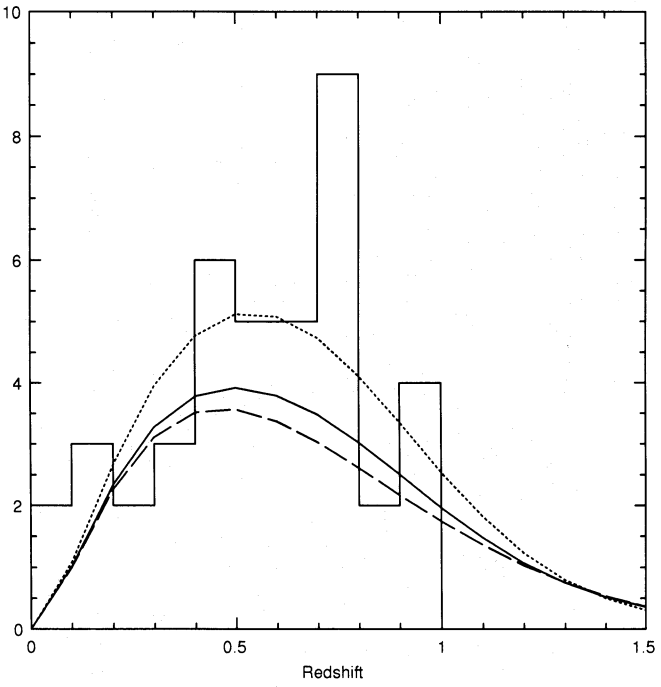

Fig. 1. Histogram of the redshift distribution of 41 $I \leq 22.1$ galaxies. (- - - - -) $q0 = 0.1$; (——) $q0 = 0.5$; (— —) $q0 = 0.5$ flat spectrum

which this line is in our spectroscopic window). This is an indication of the importance of star formation at moderate redshift. In all but one dwarf galaxy, the interstellar medium is strongly ionized by relatively hot stars, as shown by strong [O III] 5007 Å emission lines. The strength of emission lines, combined with the quality of our data, provides intensity line ratios with relatively small uncertainties. Correction for reddening can be found in Table 3 and is derived from the Hα/Hβ ratio when Hβ in emission is present.

5.2. 1415-1027: a primordial galaxy at z= 0.21?

This galaxy is rather compact and barely spatially resolved in our images. The spectrum shows strong and highly ionized emission lines (Fig. 2), associated with a very blue and faint continuum. Emission line regions seem also very compact. The Balmer lines down to Hδ are detected and the Balmer decrement corresponds to theoretical values, which imply no or a very small amount of dust in that galaxy.

Assuming electronic densities comparable to what is found in H II regions ($n_e \simeq 100\ cm^{-3}$), one can deduce preliminary parameters of the 1415−1027 properties. [O II] 3727 Å is absent or barely detected ([O II] 3727 Å)/([O III] 4959 Å + [O III] 5007 Å) < 0.02, which means that all the gas is strongly ionized, and hence, that the effective temperature should be much higher than in normal H II regions, namely $T^* > 50\,000$ K (see Fig. 8 of McCall et al. 1985), which is also supported by the presence of He II 4686 Å. The detection of [O III] 4363 Å implies high temperatures for the gas, and the ratio ([O III] 4959 Å + [O III]5007 Å)/[O III] 4363 Å = 37 ± 13 provides $T > 18\,000$ K and a probable value of $T = 21\,000$ K (see Osterbrock 1989). Note, that again this value is significantly higher than those of H II regions (see McCall et al. 1985). Values of ([O II] 3727 Å + [O III] 4959 Å + [O III] 5007 Å)/Hβ, and [O II] 3727 Å/Hβ implies relative metallicity abundances (in terms of solar abundances) less than 0.2 and 0.1, respectively (see Fig. 9 and Tables 12 and 13 of McCall et al. 1985). These limits are also compatible with the negative detection of [S II] 6725 Å and [N II] 6583 Å emission lines. From the code PHOTO described by Stasinska (1990), we estimate that the effective temperature should exceed 55 000 K while the metallicity abundance should be lower than 0.05 times the solar value. One might favor lower estimates for gas and effective temperatures, by accounting for strong collisional de-excitation which would occur in an interstellar medium much denser than in a typical H II region (Osterbrock 1989). Unfortunately, estimates of the electronic density are difficult for such a faint object. However, the blue slope of the continuum ($B - V \simeq -0.3$ at rest), without a decrease even below 4000 Å at rest, suggests high effective temperatures (O and possibly WR stars), which are also required to provide a much higher He II 4686 Å/He I 4471 Å ratio ($\simeq 3$) than in any H II regions. On the other hand, the small metallicity abundance and the absence of dust might impede cooling mechanisms and hence explain values of the electron temperature as high as 21 000 K. The large Hβ equivalent width, $W_{\lambda, H\beta} = 272 \pm 30$ Å, means that as much as 50 ± 10% of the continuum at 4860 Å is provided by gas

Table 3. Emission line properties of the 6 dwarf galaxies

Galaxy	z	L/L^*	Hα/Hβ	Extinction	Notes
1415−2632	0.067	0.009	Hβ not detected	—	Interaction
0958−1281	0.111	0.01	Hβ in abs.	—	—
0300−726	0.135	0.014	Hβ not detected	—	Merging
1415−1027	0.208	0.025	2.5 ± 0.5	0	Forming galaxy
1415−726	0.233	0.025	4 ± 1	0.82	Possible interaction
1415−164	0.081	0.047	4.6 ± 0.4	1.2 ± 0.2	Merging

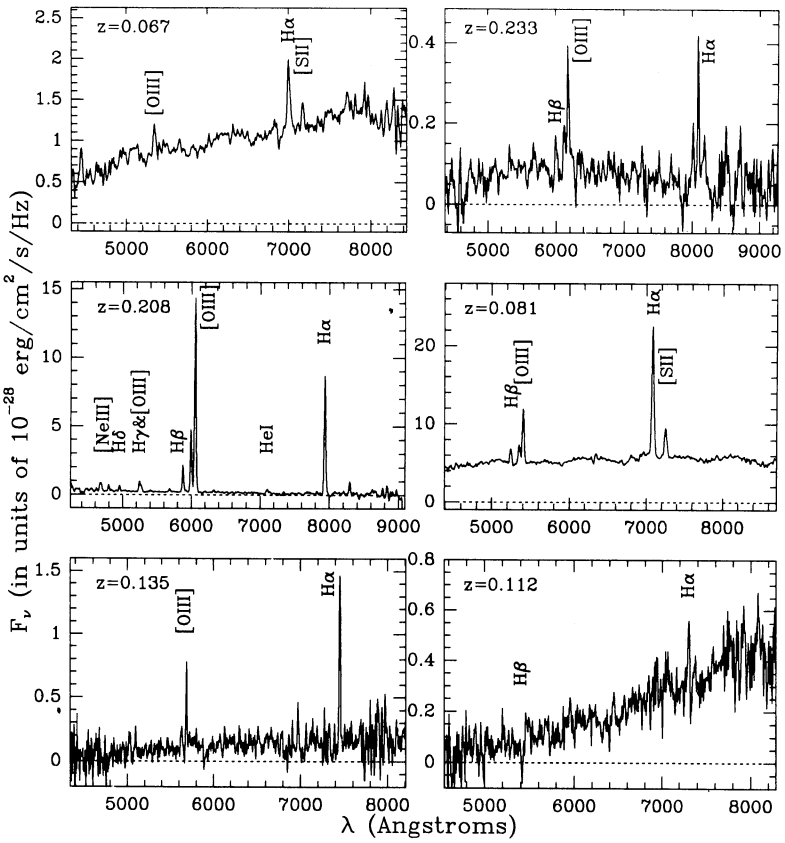

Fig. 2. Spectra of the 6 dwarf galaxies detected in our sample, from top to bottom, left to right: 1415−2632, 1415−726, 1415−1027, 1415−164, 0300−726 and 0958−1281

recombination processes. The extremely high equivalent width of Hα ($W_{\lambda,\mathrm{H}\alpha} = 2860 \pm 1000$ Å) is consistent with the fact that, at 6565 Å, the continuum could be entirely due to the gas, while the contribution of (relatively cold) stars should be smaller than 30%.

This analysis suggests that a very recent starburst ($< 10^7$ yrs) of very or extremely hot stars is occurring in 1415−1027, in a medium having a very low metallicity abundance (<0.1 solar). There is no evidence for the presence of older stars, and although we cannot rule out the presence of any of them, we believe that 1415−1027 is forming its first generation of population II stars. It could be even more primordial than ESO 400-G43, which was proposed as a forming galaxy by Bergvall & Jorsater (1988).

5.3. *Starburst induced by merging*

The merging hypothesis for starburst galaxies can be tested by a careful examination of their images and of their two dimensional spectra centered on the strongest emission lines. Three dwarfs (1415−2632, 1415−164 and 0300−11) among 6 are probably in a merging process which presumably triggers the star formation. The three objects have the strongest emission line activity among the dwarfs of our sample apart from 1415−1027. They exhibit large reddening and relatively strong [S II] 6725 Å emission lines, and hence are probably relatively old objects in which stellar activity has (recently) occurred.

1415−164 looks like an edge-on spiral with a faint object embedded in the outer part of the disk (Fig. 3a), while Hα and [O III] 5007 Å emissions present two well separated peaks (see Fig. 3a). The main one lies $2h_{50}^{-1}$ kpc from the disk center, while the secondary one lies further, near the edge of the disk ($3.6h_{50}^{-1}$ kpc from the center). The difference in radial velocity between the two components is lower than 80 km s^{-1}. 1415−164 seems to show the interaction of an extremely small dwarf and a spiral dwarf, and both present starburst activity near the encounter point. The main component has an emission-line spectra (after correction for reddening) very similar to NGC 454 west which is a blue irregular in a merging process (see Johansson 1988). We then interpret it as a recent starburst ($< 10^7$ yrs) superimposed to an underlying old star population ($W_{\lambda,\mathrm{H}\alpha} = 94 \pm 5$ Å). Merging probably induces a starburst activity in both components, and possibly disrupts the disk of the main component at the position of the fainter component.

In 1415−2632, the peak of the Hα emission is shifted from the galaxy center by, ∼0″.6 (or 1 kpc, see Fig. 3b). The galaxy shows a faint companion, 4 kpc to the SE (Fig. 3b). In 0300−726, the [O III] 5007 Å and Hα lines show a double structure (Fig. 3c) which indicates two emitting spots 1.8 kpc and 330 km s^{-1} apart. Another case of interaction is suspected in 1415−726 from the presence of a faint companion 2.2″ SE on the direct images (Fig. 3d), but we cannot assess if it is at the same redshift since it was not included in the slit.

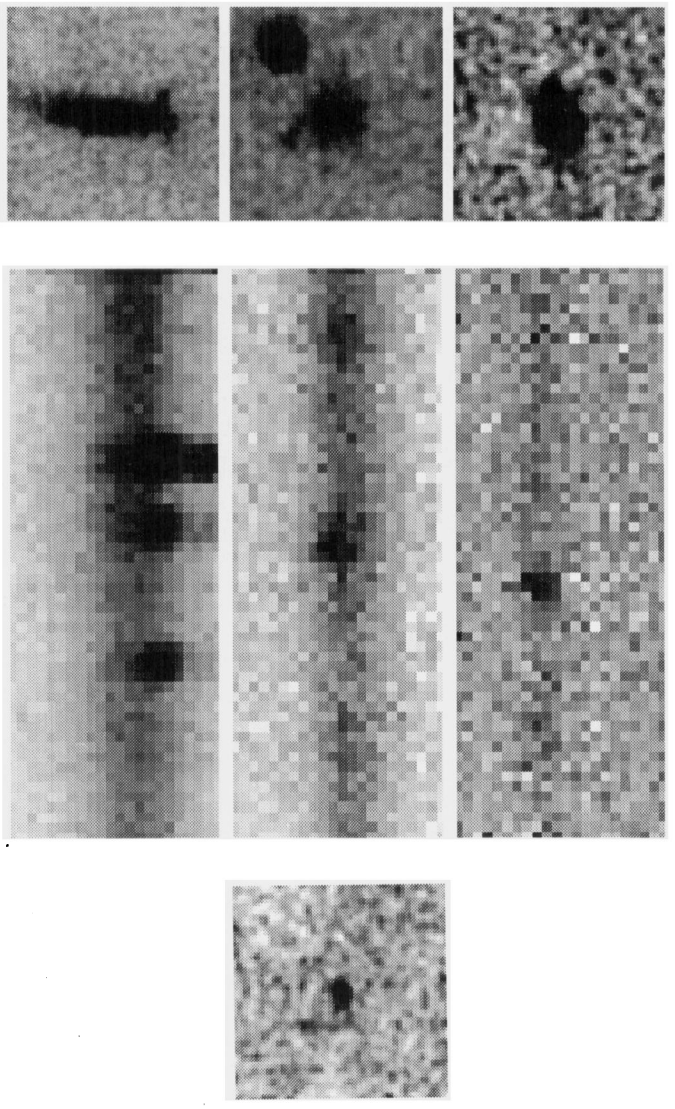

Fig. 3. Imaging and 2D spectral information. (a1) Galaxy 1415−164, *I* band image, seeing 0″9 FWHM; (a2) galaxy 1415−164, 2D spectrum enlarged around the Hβ and [O III] lines; (b1) galaxy 1415−2632, *I* band image, seeing 0″9 FWHM; (b2) galaxy 1415−2632, 2D spectrum enlarged around the Hα line; (c1) galaxy 0300−726, *I* image, seeing 0″8 FWHM; (c2) galaxy 0300−726, 2D spectrum around the Hα line; (d) Galaxy 1415−726, *I* image, seeing 0″9 FWHM

6. Discussion and conclusion

The redshift distribution of our sample of 44 galaxies brighter than $I=22.1$ is consistent with no or minimal evolution of their average properties (number and luminosity). However, the local luminosity function is not a good fit to their distribution. At low-*z*, there is a significant excess of dwarf galaxies ($L \leq 0.05L^*$) which, combined with a slight under-abundance of bright galaxies at large *z* (no galaxies beyond $z=1$), provides the apparently non-evolved properties of the sample (red counts, average redshift and number density). A comparison with the results of Cowie et al. (1992) imply that the bluest faint galaxies ($B-I \leq 1.9$) have smaller redshifts on average than the reddest ones. Colors and over-abundance of these dwarfs are good indications that they belong to the same population of low-redshift and low-luminosity galaxies, which Cowie et al. (1992) suggested to be responsible for the blue excess of the counts.

Although our sample is selected on the basis of the light from the old stellar content of galaxies, all the dwarfs found show signs of star formation activity. This suggests that this phenomenon was still very common at low redshift ($z=0.1$–0.2). This result would stand, even if all the unidentified objects were non-active dwarfs at low redshift (which would moreover imply an even larger excess of dwarfs). All the mechanisms invoked by several authors (Broadhurst et al. 1988; Guiderdoni & Rocca 1990; Lilly et al. 1991) to explain the global properties of faint galaxies, seem to be at work in our sample. Indeed, signs of starburst activity are seen in most of the dwarfs. Among them, more than half are in a merging process which probably induces the starburst activity. We also find a galaxy which might be forming its first population II stars. This object seems to be one of the best primordial candidates found to date, and will be intensively studied in the near future.

We finally believe that the blue excess in the counts is mainly due to a significant overdensity (by a factor ranging from 3 to 10 times the local density) of blue and star forming dwarfs at relatively low redshifts. This over-abundant population seems to show a complex mixture of several evolutionary mechanisms, all being responsible for the high star formation rate within this redshift range. This indicates that only a large sample of more than 1000 galaxies could provide enough constraints on how galaxies evolved and even were formed. High S/N ratios are also required and are attainable, even with low resolution spectroscopy, for the analysis of the strong emission line galaxies at moderate redshifts. Such a sample has the potential to provide estimates of the metallicity and dust abundances, temperatures and age, which all are crucial quantities for our understanding of the different physical processes involved, and of their relative importance.

Acknowledgements. We thank L. Cowie, S. Lilly, M. McCall, D. Péquignot, and G. Stasinska for useful discussions. The RVSAO correlation programs and the photoionization code were kindly made available by D. Mink at the CfA, Harvard and G. Stasinska at Paris-Meudon Observatory.

References

Bergvall N., Jorsater S., 1988, Nat 331, 589
Binggeli B., Sandage A., Tammann G.A., 1988, ARA&A 26, 509
Broadhurst T.J., Ellis R.S., Shanks T., 1988, MNRAS 253, 686
Colless M.M., Ellis R.S., Taylor K., Hook R.N., 1990, MNRAS 244, 408

Colless M.M., Ellis R.S., Broadhurst T.J., Taylor K., Peterson B.A., 1992, preprint
Cowie L.L., Songaila A., Hu E.M., 1991, Nat 354, 460
Efstathiou G., Ellis R.S., Peterson B., 1988, MNRAS 232, 431
Guiderdoni B., Rocca-Volmerange B., 1990, MNRAS 247, 166
Johansson L., 1988, A&A 191, 29
Le Fèvre, Bijaoui A., Mathez G., Picat J.P., Lelièvre G., 1986, A&A 154, 92
Lilly S.J., 1992, preprint
Lilly S.J., Cowie L.L., Gardner J.P., 1991, ApJ 369, 79
McCall M., Rybski P.M., Schields G.A., ApJS 57, 1
Oke J.B., 1974, ApJS 27, 21
Osterbrock D.E., 1989, Astrophysics of gazeous nebulae and active galactic nuclei. University Science Books
Stasinska G., 1990, A&AS 83, 501
Tyson J.A., 1988, AJ 96, 1